

# A study of pressure pulses generated by travelling bubble cavitation

By SANJAY KUMAR† AND CHRISTOPHER E. BRENNEN

California Institute of Technology, Pasadena, CA 91125, USA

(Received 3 January 1992 and in revised form 3 May 1993)

The collapse process of single bubbles in travelling bubble cavitation around two axisymmetric headforms have been studied acoustically to understand the collapse process of a cavitation bubble and characterize the sound emission in travelling bubble cavitation. The bubbles were observed to collapse and then sometimes to rebound and collapse again, resulting in one or two pulses in the acoustic signal from a cavitation event. It was observed that each of the pulses could contain more than one peak. This phenomenon is called multipeaking and is clearly distinct from rebounding. The occurrence of rebounding and multipeaking and their effects on some characteristic measures of the acoustic signal such as power spectra are examined in this paper. Two particular headforms (ITTC and Schiebe) with distinct flow characteristics were investigated.

Both rebounding and multipeaking increased with reduction in the cavitation number for the ITTC headform. Smaller flow velocity, smaller cavitation number and multipeaking delay the rebound. The peak amplitude of the sound emitted from the first collapse was seen to be twice as large as the peak amplitude of sound from the second collapse, suggesting a repeatable process of bubble fission during the collapse process. Multipeaking and rebounding increased the characteristic measures of the acoustic signal such as the acoustic impulse. These characteristic measures have larger magnitudes for smaller flow velocity. Also, the values of these characteristics are larger for the ITTC headform than for Schiebe headform.

Theoretical calculations based on the Rayleigh–Plesset equation were seen to correctly predict the order of magnitude of most of these characteristic measures. However, the distribution of spectral energy is not properly predicted; bubble fission during the collapse is thought to account for this discrepancy. Reduction in the cavitation number and multipeaking are observed to decrease the fraction of spectral energy contained in the high-frequency range (30–80 kHz).

---

## 1. Introduction

A free-stream nucleus grows into a large cavity when it migrates into low-pressure regions in a flow and stays there long enough to permit growth. It will collapse violently upon migration into flow region of higher pressure and this collapse results in sound emission and in damage to the solid surfaces nearby. This phenomenon is termed bubble cavitation and is a major source of noise and damage in ship propellers, hydrofoils and turbomachines; it may also affect the performance by altering the flow. Hence understanding of bubble cavitation is important for designing these machines.

† Present address: Room 2-336, Massachusetts Institute of Technology, Cambridge MA 02139, USA.

The dynamics and acoustics of travelling bubble cavitation have been extensively studied both experimentally and theoretically for many years. Most of the theoretical work has focused on modifications of the Rayleigh equation for a spherically collapsing cavity. Plesset contributed a substantial body of work in this area and Gilmore (1952) included compressible effects. Deviations from the spherical geometry due to the presence of a wall and the resulting shape deformations were investigated by Plesset & Chapman (1971) and more recently by Blake, Taib & Doherty (1986). Fitzpatrick & Strasberg (1956) proposed using the Rayleigh–Plesset equation in combination with the pressure history in the flow to calculate the bubble radius and the resulting noise from the collapse process. Benjamin (1958) related the presence of  $f^{-2}$  variation ( $f$  being the frequency) in the power spectra of the resulting noise to the generation of shocks due to effects of compressibility during the bubble collapse process. This research has been summarized in the review by Plesset & Prosperetti (1977).

Early experiments measured the cavitation noise generated in a venturi (Harrison 1952) and by stirring rods (Mellen 1954). Photographic and acoustical studies of the collapse of a spark- or laser-generated cavity in a quiescent liquid have also been conducted by a number of researchers including Harrison (1952), Mellen (1956) and, more recently, Lauterborn & Bolle (1975), Kimoto (1987) and Vogel, Lauterborn & Timm (1989). Photographic studies in such quiescent environments have revealed the presence of a re-entrant jet, as first seen in studies by Naudé & Ellis (1961). Fundamental considerations in the mechanism of jet formation have been discussed well in the elegant paper by Benjamin & Ellis (1966). Vogel *et al.* (1989) have also photographed shock waves resulting from the collapse of such cavities, thus confirming the importance of the effects of the liquid compressibility.

Only a few researchers, notably Knapp & Hollander (1948), Ellis (1952), Blake, Wolpert & Geib (1977), Hamilton (1981), Hamilton, Thompson & Billet (1982), Marboe, Billet & Thompson (1986) and Ceccio & Brennen (1991) have studied the collapse of hydrodynamically generated cavitation bubbles. These studies show that cavitation bubbles are usually hemispherical (Knapp & Hollander 1948; Ellis 1952). Blake *et al.* (1977) photographed the collapse of cavitation bubbles over a tripped hydrofoil and observed that the bubble deforms into a hemispherical shape before collapsing and that it breaks up into pieces during the collapse process. A similar pattern of bubble breakup has been observed photographically in travelling bubble cavitation around axisymmetric headforms by Ceccio & Brennen (1991). Van der Meulen & van Renesse (1989) have acoustically and photographically studied the collapse of laser-produced cavities in flows around hemispherical headforms.

Mellen (1954, 1956) made measurements of the spectra of noise produced by a collapsing cavity and of the cavitation noise produced by stirring rods. The noise generated by hydrodynamic cavitation has been measured by Hamilton (1981), Hamilton *et al.* (1982), Marboe *et al.* (1986), and Blake *et al.* (1977). Arekeri & Shanmuganathan (1985) used spectra measurements to determine the value of the void fraction above which interactive effects between bubbles became important. Many researchers have suggested treating the noise pulses as a stochastic process (Morozov 1969; Illichev & Lesunovskii 1963; and Baiter 1974) and using the noise generated by a single collapsing bubble to synthesize the spectra of the noise generated by travelling bubble cavitation (Baiter 1986).

Some of the earliest studies of a single cavitation bubble observed the bubble collapsing, growing and collapsing again (Knapp & Hollander 1948). Harrison (1952) traced the origins of the rebound to the presence of permanent gas in the bubble. Since

that time rebounding has been observed in both flow-induced cavitation and in the collapse of spark- or laser-produced cavities. Rebounding generates two or more pressure pulses separated by an intermediate growth phase. Another phenomenon called *multipeaking* can be seen in the acoustic signal generated by the collapse of spark-produced cavities Mellen (1956; and Teslenko 1980). Ceccio & Brennen (1991) also observed multiple-peaked pulses in the noise from single events.

Thus *rebounding* and *multipeaking* are seen to be characteristic features of the noise generated by collapse of a bubble. The present investigation examines these characteristic features as well as their impact on cavitation noise. The dependence of multipeaking and rebounding on flow conditions as represented by cavitation number, flow velocity and to a limited extent on the local flow structure has been investigated in order to understand the collapse mechanism in travelling bubble cavitation. The results are compared to calculations using the Rayleigh–Plesset equation in a manner similar to that proposed by Fitzpatrick & Strasberg (1956). It is hoped that the information generated by such an investigation can be used in a model similar to the one suggested by Baiter (1986) to construct the spectra of travelling bubble cavitation.

## 2. Experimental details

The experiments were conducted in the low turbulence water tunnel (LTWT) at the California Institute of Technology with experimental equipment similar to that used by Ceccio & Brennen (1991). The test section of the LTWT is 30.5 cm × 30.5 cm and 2.5 m long. The test section velocity  $U$ , can be varied in the range 0–10 m/s with maximum free-stream turbulence of less than 0.05%. A full description of the LTWT has been given by Gates (1977). All the experiments were conducted at a fixed flow velocity, the desired cavitation number being obtained by lowering the static pressure in the water tunnel. The air content was measured by a Van Slyke apparatus and was maintained between 8 and 10 p.p.m.

Travelling bubble cavitation was produced on the two axisymmetric headforms used by Ceccio & Brennen (1991), namely a Schiebe headform of diameter 5.08 cm (Gates *et al.* 1979) and an ITTC headform of 5.59 cm diameter (Lindgren & Johnsson 1966). The Schiebe headform was designed to suppress laminar separation in cavitating conditions (Schiebe 1972). It produces a sharp pressure drop with a minimum pressure coefficient of  $-0.75$  (figure 1). The ITTC possesses a laminar separation region. It has a relatively smooth pressure drop with a minimum pressure coefficient of  $-0.62$  (figure 1). The pressure coefficient,  $C_p$  is defined as  $(P_s - P_o)/\frac{1}{2}\rho U^2$ .  $P_o$  and  $U$  are free-stream pressure and velocity,  $\rho$  is the density of water and  $P_s$  is the local pressure on the surface of the headform. The headforms were made of lucite whose acoustic impedance is close to that of water (Ceccio & Brennen 1991). An ITC-1042 hydrophone was placed in the headform interior, which was filled with water (figure 2). This allows relatively reverberation-free recording of the initial portion of the acoustic signal generated by the cavitation on the surface of the headform. A collapsing bubble is a sound source of monopole type and the sound gets weaker away from the source. Thus reverberation from the tunnel walls reaching the hydrophone is considerably weaker than the original acoustic emission. This means that since the cavitation site is much closer to the hydrophone than it would be if the hydrophone were placed near tunnel walls, the distortion of the signal due to the natural acoustic modes of water tunnel and the acoustic reflections from the water tunnel walls are minimized. While the acoustic path between the bubble and the hydrophone is not perfectly transparent, Ceccio & Brennen (1991) found this distortion to be insignificant by comparing the signal with that of a

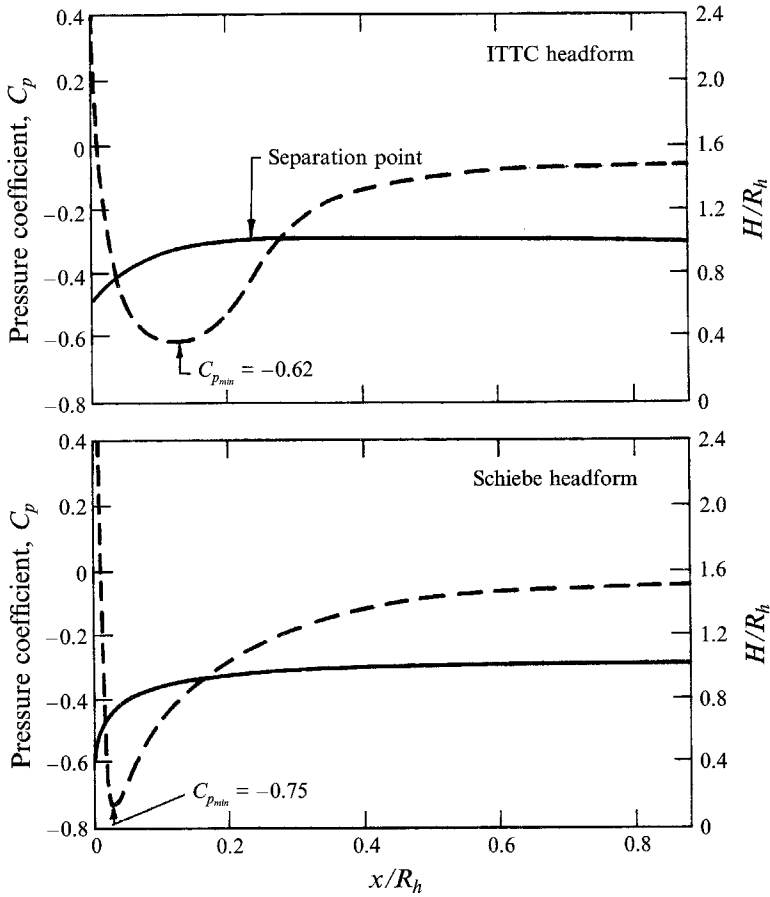


FIGURE 1. Pressure distributions on the ITTC and Schiebe headforms.

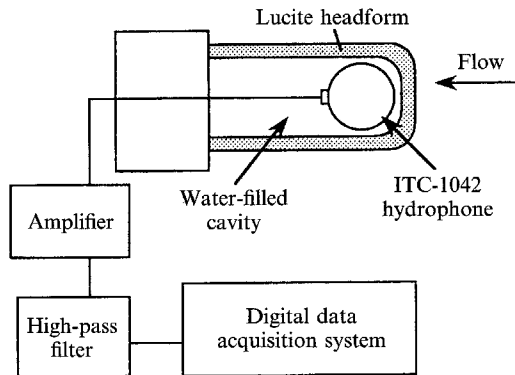


FIGURE 2. Schematic illustrating the instrumentation of the headform.

far-field hydrophone. Kuhn de Chizelle (1993) and Kuhn de Chizelle *et al.* (1992) carried out reciprocity measurements over the range 1 to 100 kHz using a similar internal hydrophone and a wall-mounted external hydrophone, and encountered a maximum discrepancy of less than 3 dB.

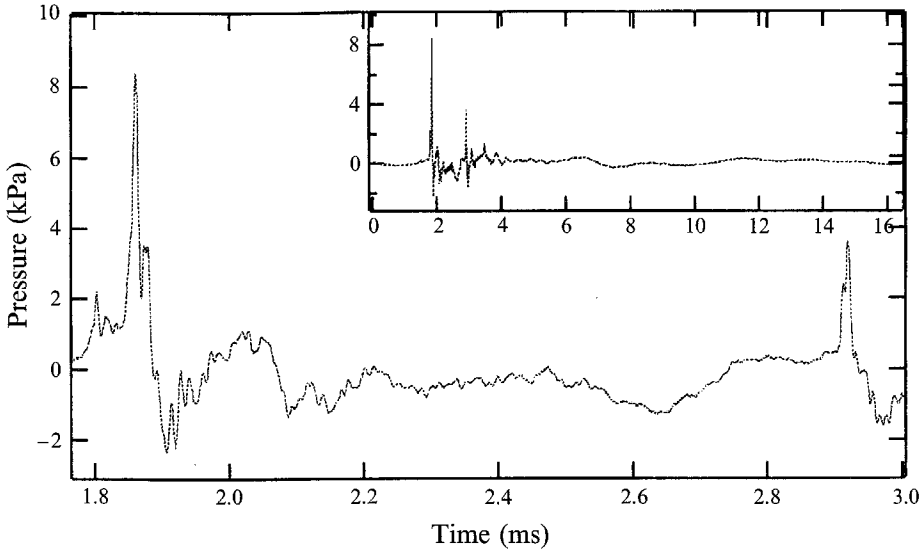


FIGURE 3. A typical amplified and filtered signal for a single cavitation event illustrating multiple peaks and a rebound. Inset shows the complete acoustic trace.

The signal from the hydrophone was amplified and extremely low frequencies ( $\ll 1$  Hz) were removed by a high-pass filter. The filtered signal was then digitally sampled at 500 kHz. It should be noted that the hydrophone has a corner frequency of 80 kHz. Therefore, the sampling rate of 500 kHz is more than sufficient to capture the detail of the acoustic signal detected by the hydrophone. Thus, for example, the peak amplitudes are meaningful and do not differ appreciably from the actual peak amplitudes measured by the hydrophone. The overlapping signals generated by a number of bubbles collapsing next to the headform almost simultaneously have been eliminated by the software used to process the acoustic data. Around 500 acoustic traces were collected for each of six operating conditions comprising three cavitation numbers (0.45, 0.50 and 0.55) and two flow velocities (8 and 9 m/s). The cavitation number,  $\sigma$ , is defined as  $(P_o - P_v)/\frac{1}{2}\rho U^2$ , where  $P_v$  is the vapour pressure at operating temperature. Cavitation under these conditions consisted only of travelling bubble cavitation. No other form of cavitation such as attached cavities were visually found on the headform. The duration of the recording was adjusted to capture the complete acoustic trace from an individual bubble collapse. A typical acoustic trace is shown in figure 3 and a sketch illustrating the definition of some of the evaluated quantities is included as figure 4. These records were digitally processed in the following way. First, peaks were detected and classified as belonging to the main pulse or the rebound pulse. Then quantities such as the peak amplitude and the time interval between the peaks were evaluated. In addition, the following quantities were evaluated:

$$I_m = \int_{t_1}^{t_2} p \, dt, \tag{1}$$

$$I_s = \int_{t_1}^{t_2} p^2 \, dt, \tag{2}$$

$$\tau_w = t_1 - t_2. \tag{3}$$

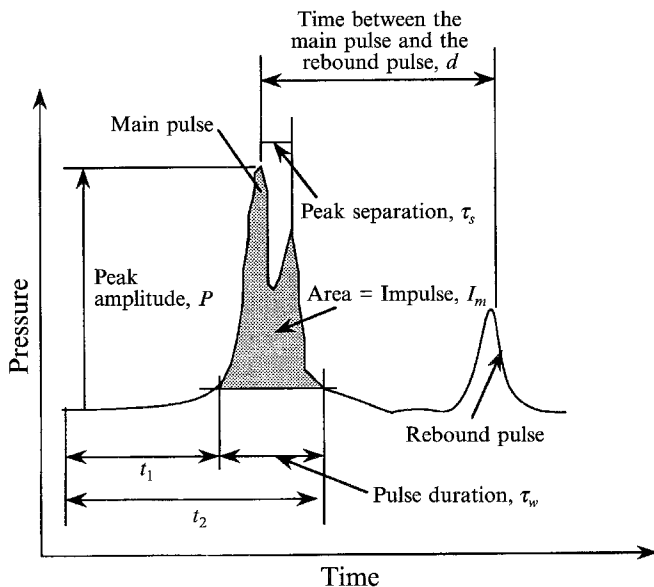


FIGURE 4. Sketch of a typical acoustic trace with the definitions of some measured quantities.

Here  $p$  is the pressure emitted from the collapsing bubble as measured at the hydrophone,  $I_m$  is the acoustic impulse, and  $t_1$  and  $t_2$  are the times of the beginning and the end of the main pulse (or the rebound pulse). The integral,  $I_s$ , is an alternative measure of the strength of the pulse and  $\tau_w$  is the duration of the pulse. Also measured were the time between the maximum peaks in the main and the rebound pulses,  $d$ , and the ratio of maximum amplitude in the main pulse to the maximum amplitude in the rebound pulse,  $r$ .

### 3. Experimental results

#### 3.1. Occurrence of multipeaking and rebounding

First, the probabilities of occurrence of the phenomena of rebounding and multipeaking were examined statistically in order to gain some insight into these phenomena. The dependence of these probabilities on cavitation number,  $\sigma$ , and to a limited extent on flow velocity are presented in figure 5 for both headforms. Consider first the phenomena of multipeaking in the main pulse. The following trends can be clearly seen from the data of figure 5. First note that changing the flow velocity from 8 to 9 m/s has little effect on the results. This is not surprising since the change in velocity is small (significantly different velocities could not be obtained due to operational limits on this water). Van der Meulen & van Renesse (1989) also found the flow velocity to have very little effect on details of the bubble collapse process. Second, the probability of rebounding increases as the cavitation number is reduced and this appears to be the case for both the headforms. It is particularly evident that rebounding almost never occurs for the highest of the three cavitation numbers tested,  $\sigma = 0.55$ . The probability of occurrence of both multipeaking and rebounding is higher for the ITTC headform than for the Schiebe headform. For the ITTC headform, the probability of occurrence of double-peaked events is almost independent of  $\sigma$ . Events with more than two peaks almost never occur with the Schiebe headform. The

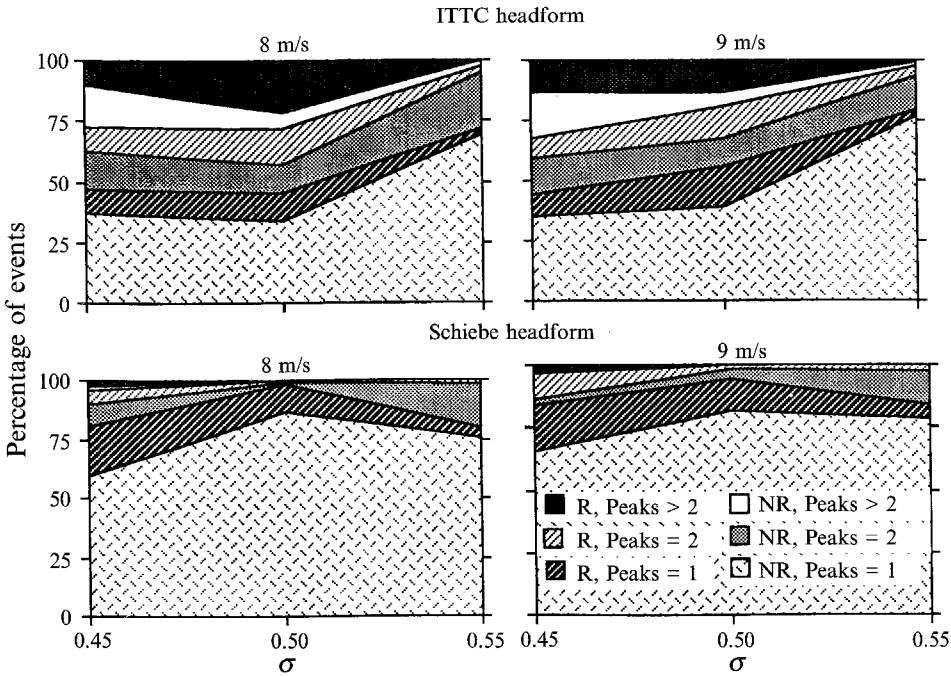


FIGURE 5. Probabilities of different types of cavitation events on the ITTC and Schiebe headforms indicating the occurrence of multiple peaks or a rebound. R and NR respectively denote events with and without rebound. The number alongside indicates the number of peaks in the main pulse.

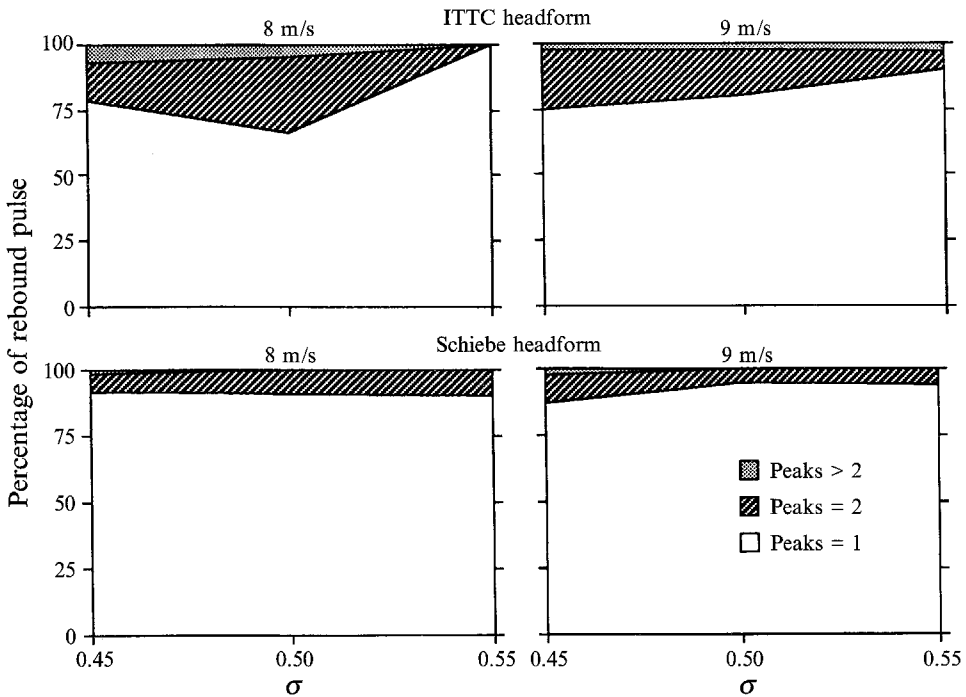


FIGURE 6. Probabilities of numbers of peaks in the rebound pulse for cavitation events on the ITTC and Schiebe headforms. The legend indicates number of peaks in the rebound pulse.

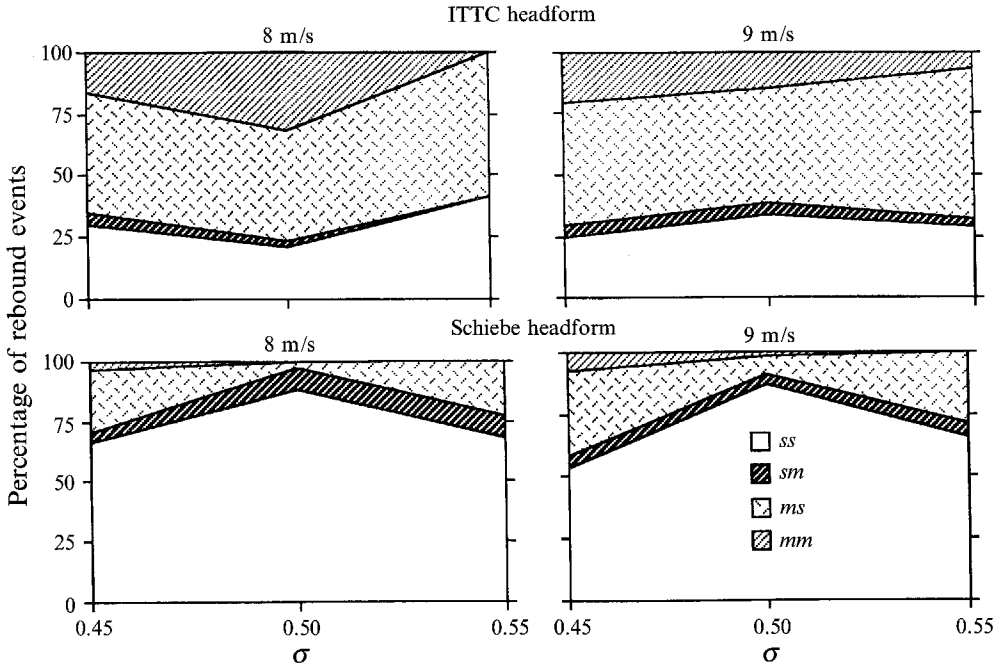


FIGURE 7. Probabilities of different types of cavitation events with rebound for the ITTC and Schiebe headforms. A two-letter symbols is used to classify the event, with the first letter indicating the number of peaks in the main pulse and the second letter the number of peaks in the rebound pulse; *s* indicates single peak and *m* indicates more than one peak.

probability of double-peaked events appears to be minimum at the intermediate cavitation number of 0.5 for the Schiebe headform. The probability of occurrence of multi-peaking in the rebound pulse was also examined and exhibited trends similar to those in the main pulse. As seen in figure 6, rebounds are predominantly single peaked (approximately 80% for the ITTC headform and 90% for the Schiebe headform).

It is convenient to classify the cavitation events with a rebound by a combination of two letters, where the first letter represents the number of peaks in the main pulse and the second letter represents the number of peaks in the rebound pulse. We use the letter *m* to denote multiple peaks and *s* to denote a single peak. The probability of occurrence of different kinds of events is shown in figure 7. It can be seen that ITTC headform has mostly *ms*-type events (50%) but *mm*- and *ss*-type events are also present in significant numbers (25%). The Schiebe headform has mostly *ss*-type events with *ms*-type events also present about 20% of the time. It is observed that *sm* events are rare, indicating that a multi-peaked rebound pulse is unlikely if the main pulse is single peaked.

Clearly, the two headforms produce characteristically different events because of the differences in the interaction between the bubble dynamics and the flow structure. The rebound pulse indicates a second collapse separated from the first collapse by a growth phase. Van der Meulen & van Renesse (1989) have related the rebounding of the bubble to its distance from the headform. In their study of the collapse of laser-produced cavities around hemispherical headforms, the bubbles very close to the headform (distance/maximum radius < 0.7) were observed not to rebound. Thus the pattern of rebounding may be governed by the distance between the growing nuclei and the headform. Owing to presence of boundary-layer separation of the ITTC headform, nuclei will be farther from the surface than on the Schiebe headform which does not



have boundary-layer separation. Therefore van der Meulen & van Renesse's (1989) observation is consistent with the present one of a greater probability of rebounding with the ITTC headform than with the Schiebe headform.

Multipeaking, however, could be the result of several mechanisms as follows:

(i) Multiple peaks may be the result of multiple pressure waves emitted during the bubble collapse process. In the present experiments, the peak separation was roughly 0.015 ms. This value will be compared to the values available in literature to understand possible mechanisms for multipeaking. Collapsing cavities have been observed to generate microjets (Kimoto 1987; van der Meulen & van Renesse 1989; Vogel *et al.* 1989). Kimoto (1987) has separately measured the pulse resulting from microjet impact and the subsequent pulse generated when the remnant cloud of smaller bubbles collapses in his study of collapse of a spark-induced cavitation bubble. The remnant cloud shock was found to be about 3 times stronger than the microjet shock and the time between them was about 0.050 ms. Vogel *et al.* (1989) have extensively studied the collapse of a laser-induced cavitation bubble. Two shock waves were photographed immediately following a non-spherical bubble collapse (their figure 15); however, no time information concerning the acoustic emission from these shocks is reported in that paper. In the same paper, the jet and the counterjet appear within 0.050 ms of the collapse (from photographs; a more accurate value is not possible because of the framing rate of 20000/s and lack of simultaneous acoustic signature). The study of the collapse of laser-produced bubbles in the flow next to a headform by van der Meulen & van Renesse (1989) comes closest to the present experiments. The jet and counterjet produced almost simultaneously (within 0.020 ms) with the first collapse of the bubble photographed in this study can also account for multiple peaks. Considering these results, the jet and counterjet produced during the bubble collapse may account for the multiple number of peaks. Van der Meulen & van Renesse (1989) observed that the production of a counterjet was enhanced for larger distances between the bubble and the surface of the headform. This may explain the greater degree of multipeaking for the ITTC headform (where bubbles may travel farther away from the surface of the headform because of presence of laminar separation) than for the Schiebe headform.

(ii) Cavitation bubbles can break up into several pieces while collapsing (as seen by Ceccio 1990) and therefore generate two or more peaks. The bubble may break up during the collapse due to shear in the flow or as a result of the onset of large bubble oscillations. From the photographs of Ceccio (1990) one can estimate the two pieces to be 1 mm apart which, at a flow velocity of about 10 m/s, would lead to peaks roughly 0.1 ms apart. This is substantially larger than the observed peak separation of about 0.015 ms.

(iii) Volume oscillations during the collapse process could cause multiple peaks. Since, the natural period of oscillation for a 20  $\mu\text{m}$  bubble is about 0.015 ms (which is consistent with the observed peak separation), volume oscillations during the collapse are a plausible explanation for multiple peaks. The natural oscillations of the bubble can be caused by the strong pressure gradient that the bubble experiences while travelling next to the headform.

It is not possible to be conclusive about the mechanism for multipeaking on the basis of the above results alone; a high-speed film simultaneous with the acoustic recording is required.

The above variations in the probabilities of multipeaking and rebounding are probably governed by the size distribution of the nuclei and by the manner in which the nuclei enter the low-pressure zone around the headform. Distinctly different

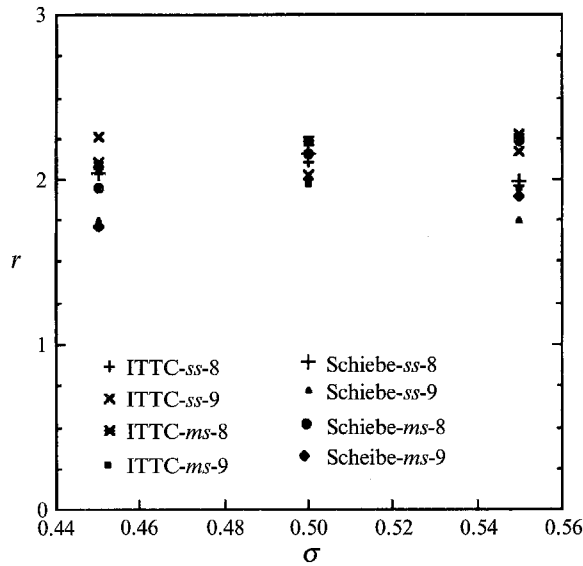


FIGURE 8. Ratio of the peak pressure amplitude of the main pulse to the peak pressure amplitude of the rebound pulse,  $r$ , as a function of the cavitation number. The legend indicates the headform, the type of events and the flow velocity.

pressure distributions (figure 1) and the presence (absence) of a laminar separation layer cause the differences in travelling bubble cavitation around the ITTC and the Schiebe headforms by influencing the trajectory of bubble travel and the pressure history experienced by the bubble while travelling along that trajectory.

### 3.2. Some characteristic measures of the acoustic signal

We now turn to other statistical features in the acoustic signal by first examining the mean value of the measured quantities. The error bars in figures 9–11 have been calculated using a 95% confidence level following Bendat & Piersol (1971). First the ratio of the maximum amplitude in the main pulse to the maximum amplitude in the rebound pulse,  $r$ , will be examined for the two velocities, for the various types of events and for the two headforms (figure 8). It is seen that most of the data are clustered around the value of 2. With a 95% confidence level, we find that the mean value of  $r$  will lie between 1.5 and 2.5. Thus, it seems that the bubble fission observed by Ceccio & Brennen (1991) happens in such a way that the second collapse (comprised of the collapse of the bubble cloud generated by the first collapse) generates only half of the maximum pressure of the first collapse. This may mean that during the first collapse certain modes of surface oscillation are excited which cause the bubble to break up in a repeatable way. Somewhat similar behaviour was observed to occur in the results for the ratio of the pulse width,  $\tau_w$ , for the first collapse to that for the second collapse. This ratio varied between 2 and 4 for the Schiebe headform and 3.5 and 8.25 for the ITTC headform. Moreover, the ratio of the impulse,  $I_m$ , for the first collapse to that for the second collapse exhibited similar behaviour. Thus, it is clear that the collapse which occurs after a rebound generates less sound than the main collapse in contrast to the observation made by Hamilton (1981).

The time between the maximum peak in the main pulse and the maximum peak in the rebound pulse,  $d$ , was also measured and exhibited a mean value between 0.5 and 1.4 ms. We have examined the classic film of Knapp entitled *Studies of Cavitation*

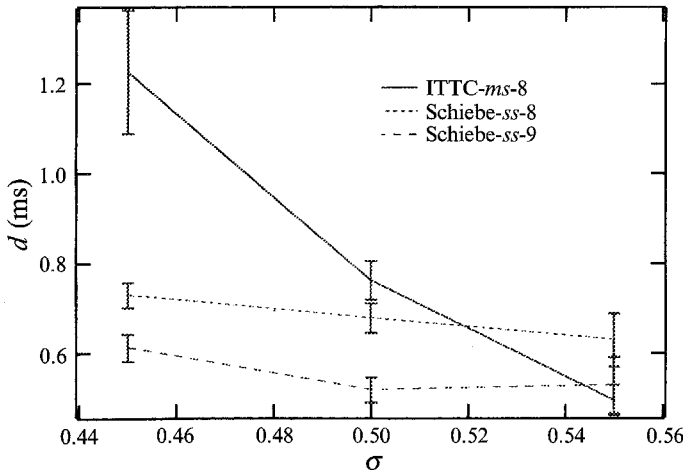


FIGURE 9. Variation of the time between the main pulse and the rebound pulse as a function of the cavitation number. The legend indicates the headform, the type of event and the flow velocity.

which shows travelling bubble cavitation around a 1.5 calibre ogive. The value of  $d$  from that film is approximately 1.5 ms which is of the same order of magnitude as the present observation. The lends confirmation to the conclusion that the two pulses in the present acoustic records are emitted by two collapses separated by a growth phase. It is observed that the value of  $d$  increased with reduction in the cavitation number and, as expected, is larger at 8 m/s than at 9 m/s for both the headforms (figure 9). Van der Meulen and van Renesse (1989) also observed delayed rebound at smaller flow velocities. Furthermore, the value of  $d$  is larger for the ITTC headform than for the Schiebe headform at both flow velocities and the smaller values of  $\sigma$  (0.50 and 0.45). The reason for this may be the larger radius of the ITTC headform which enlarges lengthscales requiring larger times between the collapses. Different pressure distribution around the two headforms have also contributed to this increase in time between two successive collapses. We should also note that multi-peaking was seen to delay the rebound for reasons which are not understood.

The quantities  $P$ ,  $I_m$ ,  $I_s$ ,  $\tau_w$  and  $\tau_s$  (called quantitative acoustic characteristics, QAC) were also examined in order to understand the effects of multi-peaking and rebounding. We consider first the variation in the mean value of the QAC with cavitation number for both headforms. The previously mentioned two-letter symbols are used to denote the types of events with a rebound. In addition, *sp* and *mp* indicates single and multi-peaked events without a rebound. It is seen from figure 10 that  $I_m$  increases with reduction in cavitation number, as can be expected. The mean values of  $P$  and  $I$  behave in a similar fashion, though the dependence of  $\tau_w$  on  $\sigma$  is quite different. The pulse width,  $\tau_w$ , has a maximum value for the intermediate cavitation numbers in most cases. Exceptions to this trend are *mp*-type events for the Schiebe headform for which the pulse width,  $\tau_w$ , decreases with decrease in the cavitation number at the flow velocity of 9 m/s and increases with decrease in the cavitation number at the flow velocity of 8 m/s. It was seen from the data that the QAC changed in similar way with the changes in the type of event, the flow velocity and the headform. Figure 10 also shows the effect of multi-peaking and rebounding on the QAC. For the ITTC headform, the mean values of the QAC for *mp*- and *ms*-type events are roughly the same and are larger than the corresponding values for *sp*-type events. In case of the Schiebe headform, the values for *sp*- and *ss*-type events are roughly the same, and are less than the values for *mp*-

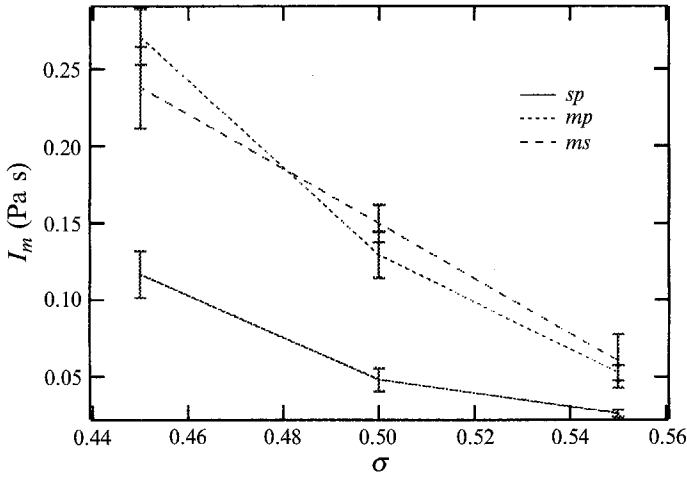


FIGURE 10. The figure illustrates the dependence of the acoustic impulse,  $I_m$ , on the type of event for the ITTC headform. The flow velocity is 8 m/s.

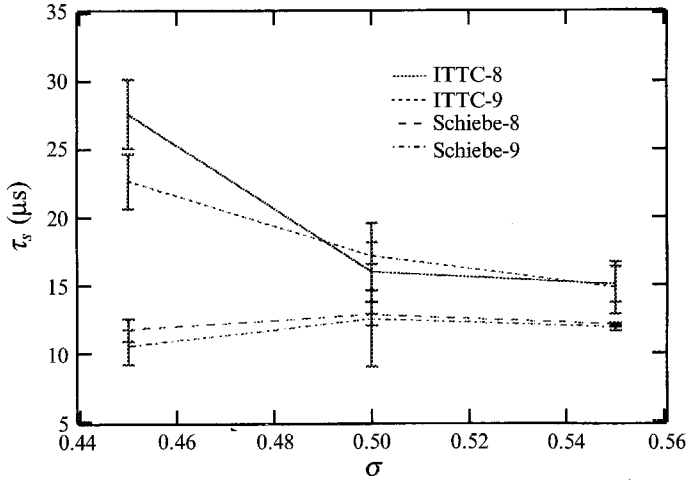


FIGURE 11. The peak separation,  $\tau_s$ , as a function of the cavitation number for each headform. The legend indicates the type of headform and the flow velocity.

type events. This pattern for the Schiebe headform can be seen only at the cavitation number of 0.45, the uncertainty in the estimate being larger at larger values of  $\sigma$ . Detailed results on variation of the QAC with the flow velocity and the type of headform are given in Kumar (1991). Figure 11 shows the variation in the peak separation,  $\tau_s$ . It remains close to 12  $\mu$ s for the Schiebe headform but increases from 15 to 23–28  $\mu$ s for the ITTC headform as the cavitation number is reduced.

### 3.3. Comparison between experimental results and theoretical calculations

To provide some benchmark with which to compare the current experimental results, the Rayleigh–Plesset equation

$$R \frac{D^2 R}{Dt^2} + \frac{3}{2} \left( \frac{DR}{Dt} \right)^2 = \frac{P_v - P_\infty(t)}{\rho} + \frac{P_{go}}{\rho} \left( \frac{R_o}{R} \right)^{3k} - \frac{4\nu DR}{R Dt} - \frac{2S}{\rho R}, \quad (4)$$

which governs the bubble radius,  $R(t)$ , as a function of the pressure variation  $P_\infty(t)$ , was integrated numerically along typical streamlines in the flow around the two headforms. Liquid properties ( $S$ : surface tension,  $\nu$ : kinematic viscosity,  $\rho$ : density and  $P_v$ : vapour pressure) for water at 300 K were used. The pressure distributions constructed used potential flow calculations and pressure distributions published by Gates *et al.* (1979) (for the Schiebe headform) and Hoyt (1966) (for the ITTC headform). The calculations assume no slip between the bubble and the flow and use a small offset from the stagnation streamline (for more detail, see Ceccio & Brennen (1991) and Kumar (1991)). They begin with upstream nuclei ranging in radius,  $R_o$ , from 2 to 400  $\mu\text{m}$ . These are assumed to be in equilibrium with the upstream flow which automatically determines the pressure of the gas ( $P_{g0}$ ) within each nucleus. Diffusion of the gas in or out of bubble is neglected and the gas is assumed to behave adiabatically with  $k = 1.4$ . The numerical calculations use a fourth-order Runge–Kutta integration scheme with variable time step which is adjusted so that the change in radius during one time step is less than 20%. This captures the details of extremely rapid, rebounding process quite accurately.

The air content is, of course, crucial to the rebounding process and therefore to the evaluation of the radiated acoustic pressure as was established by Benjamin (1958), Baiter (1982), and others. Many of those calculations begin when the bubble is at its maximum radius and therefore require assumptions regarding the partial pressure,  $P_G(R_M)$ , of the gas at that point. The current calculations do not require any such assumption; the air content is established by the equilibrium conditions upstream. However, to allow a comparison with the collapse calculations which use the parameter  $\alpha = P_G(R_M)/P_o$  (where  $P_o$  is a measure of ambient pressure) it may be noted that the *calculated* values of  $\alpha$  for bubbles which cavitate range from about  $10^{-8}$  for a 10  $\mu\text{m}$  nuclei to  $10^{-6}$  for a 100  $\mu\text{m}$  nuclei.

The radiated acoustic pressure  $p$ , is then calculated as

$$p(x, t) = \frac{\rho}{4\pi x} \frac{d^2 V}{dt^2}, \quad (5)$$

where  $V(t)$  is the volume of the bubble and  $x$  is the distance from the bubble to the point of measurement. Acoustic pressures resulting from nuclei of various sizes were calculated and used to calculate the impulse,  $I_m$ , the pulse width,  $\tau_w$  and the time interval between two successive collapses following equations (1)–(3). In these calculations,  $t_1$  and  $t_2$  were taken to be times when  $d^2 V/dt^2 = 0$  on either side of a collapse. The distance  $x$  is assumed to be  $R_h$ , the headform radius, since that is the location of the hydrophone in the experiments. To facilitate comparison these quantities are nondimensionalized as follows:

$$I^* = 4\pi I_m / \rho U R_h, \quad (6)$$

$$\tau_w^* = \tau_w U / R_h \quad (7)$$

$$d^* = dU / R_h. \quad (8)$$

Theoretical and experimental results for the ITTC headform are compared in figures 12 and 13 in which  $\tau_w^*$  and  $d^*$  are plotted against the impulse,  $I^*$ . Note that all the experimental values plotted are for the main acoustic pulse produced by the first collapse of the bubble. The solid and dashed lines indicate the values for cavitation numbers of 0.6 and 0.3 respectively and form an envelope for the theoretical results. It can be seen from figure 12 that the data points form a small cluster near the origin

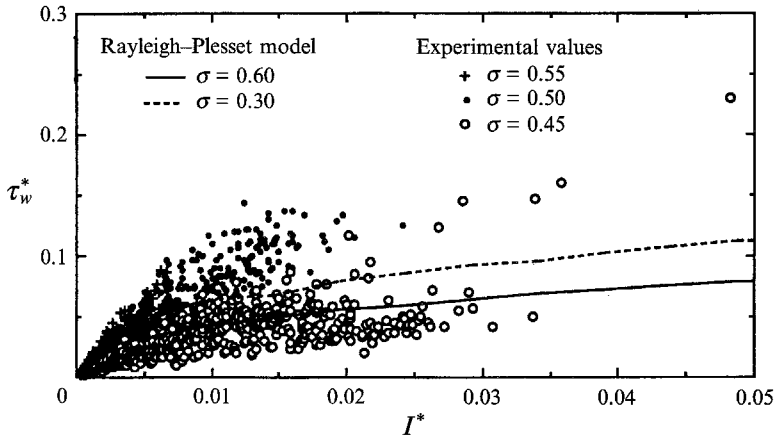


FIGURE 12. Experimentally obtained values of the non-dimensional pulse width,  $\tau_w^*$ , plotted against the non-dimensional impulse,  $I^*$ , and compared with the values from the numerical integration of the Rayleigh–Plesset Equation. The data are for the ITTC headform and different cavitation numbers. The flow velocity is 8 m/s.

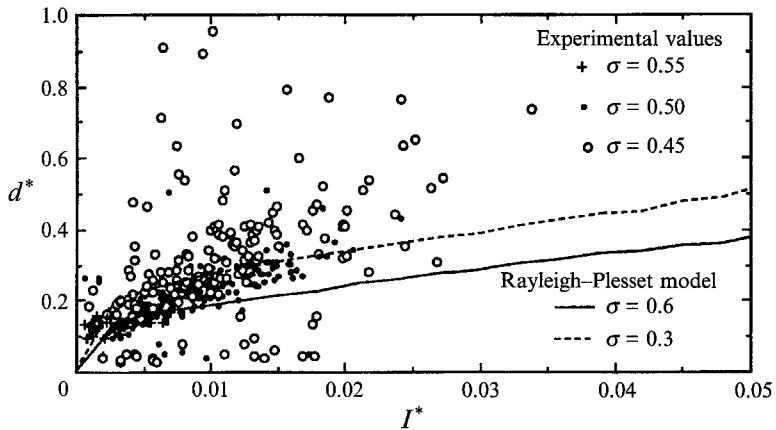


FIGURE 13. Experimentally obtained values of the non-dimensional time between the main pulse and the rebound pulse,  $d^*$ , plotted against the non-dimensional impulse,  $I^*$ , and compared with the values from the numerical integration of the Rayleigh–Plesset equation. The data are for the ITTC headform and different cavitation numbers. The flow velocity is 8 m/s.

for the cavitation number of 0.55. These values are close to the theoretical solution. This cluster becomes larger as the cavitation number is reduced to 0.50, for which most of the data points lie above the theoretical envelope. However, the cluster moves downward and rightward with larger values of  $I^*$  when the cavitation number is reduced further to 0.45. For this cavitation number most of the data lie below the theoretical values. Though the Rayleigh–Plesset equation yields results that are the right order of magnitude, it fails to predict the dependence of the pulse width,  $\tau_w^*$ , on the cavitation number. Note that  $\tau_w^*$  is halved as the cavitation number is reduced from 0.50 to 0.45, which is larger than any uncertainty in the experimental measurements.

Figure 13 shows a similar plot for the time between the first and the second collapses,  $d^*$ , as a function of the impulse,  $I^*$ . Most of the experimental values for the cavitation

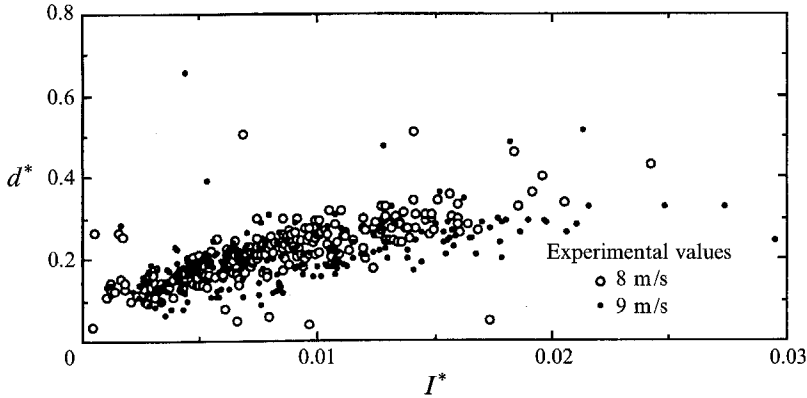


FIGURE 14. Experimentally obtained values of the non-dimensional time between the main pulse and the rebound pulse,  $d^*$ , plotted against the non-dimensional impulse,  $I^*$ . The data are for the ITTC headform, different flow velocities and cavitation number of 0.50.

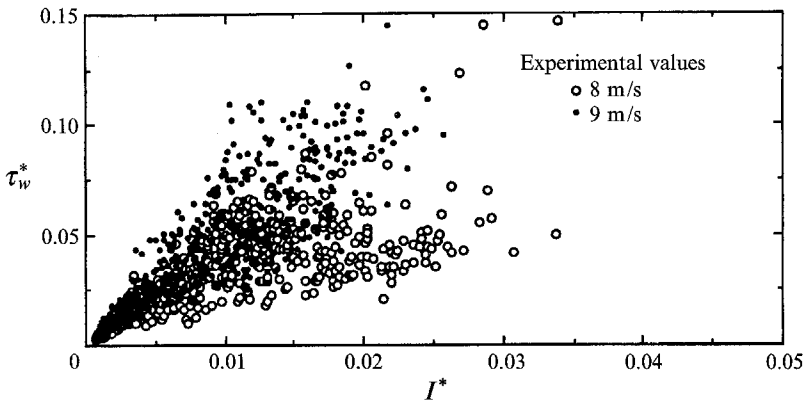


FIGURE 15. Experimentally obtained values of the non-dimensional pulse width,  $\tau_w^*$ , plotted against the non-dimensional impulse,  $I^*$ . The data are for the ITTC headform, different flow velocities and cavitation number of 0.45.

numbers of 0.55 and 0.50 lie within the theoretical envelope. However, as the cavitation number is reduced to 0.45, the data begin to exhibit a great deal of scatter for reasons which are not known.

Figures 14 and 15 illustrate the dependence of the data on the flow velocity and show that a smaller flow velocity delays the rebound (figure 14). It appears that the first and second collapses occur at specific locations on the headform (determined by the pressure distribution). Figures 7–10 of Ceccio & Brennen (1991) indicate these locations approximately. On the other hand, a larger flow velocity is seen to increase the pulse width,  $\tau_w^*$  (figure 15) and this may indicate significant relative motion between the bubble and the fluid during the collapse process.

It is noteworthy that the time between the first and the second collapse,  $d^*$ , is well correlated with the impulse,  $I^*$ , for the cavitation number of 0.50 (figure 14) and shows wide scatter for cavitation number of 0.45 (figure 13). The reasons for this are not understood.

It is clear from figures 12–15 that the present experimental data for  $I^*$ ,  $\tau_w^*$  and  $d^*$  are closer to the values predicted by the Rayleigh–Plesset model than the impulse

and maximum bubble volume data presented by Ceccio & Brennen (1991). It appears that the Rayleigh–Plesset model underestimates the maximum volume of the bubble while it predicts the right order of magnitude for the impulse,  $I^*$ , pulse width,  $\tau_w^*$ , and the time between the first and second collapse,  $d^*$ . This can be understood as follows. It is probable that a spherical collapse of a bubble produces the maximum sound emission and any departures from sphericity during the collapse reduces the amplitude of sound emitted. The Rayleigh–Plesset equation assumes spherical bubble collapse and thus underestimates the volume required to produce the same impulse. It should also be noted that the Rayleigh–Plesset equation includes only viscous dissipation and does not model the breakup of a collapsing bubble, which is a source of significant energy dissipation in our experiments. One consequence of this is that a bubble undergoes at most one rebound in our experiments while multiple rebounds are predicted by the Rayleigh–Plesset equation.

Another property of the Rayleigh–Plesset solutions is that all free-stream nuclei growth to almost the same size (Flynn 1964; Brennen & Ceccio 1989). Since the quantities  $d^*$ ,  $\tau_w^*$  and  $I_m^*$  depend upon the maximum bubble size (Ceccio & Brennen 1991), it is not surprising that they do not depend strongly on the size of the free-stream nucleus.

### 3.4. Power spectra measurement

In order to examine the spectral content of the cavitation, the hydrophone output was sampled at 1 MHz, and about 200 acoustic traces of 16384 data points each were collected for each operating condition. These data records were processed to obtain a separate record of 8192 points for each cavitation event and the resulting event records were then used to calculate the power spectra. The events were also sorted and classified according to the existence of rebounds and multi-peaking; they were then labelled by the two-letter combination used earlier. It was found that predominant events were of the *mp* and *sp* type. Thus the effect of multi-peaking on the power spectra could be meaningfully examined. The spectra presented here are the averages of all of the spectral density data for all of the individual events of the type specified. The spectra were non-dimensionalized in the following way. The sum of the ordinates lying between two frequencies in a non-dimensional spectrum gives the fraction of total spectral power emitted between those two frequencies. If the mean power spectral density is given by  $A_i$  ( $i = 1, \frac{1}{2}N + 1$ ), where  $i$  indicates a frequency of  $(i - 1)R'/N$ ,  $R'$  is the sampling rate and  $N$  is the total number of data points in the record, then  $P_s^*$  is defined as

$$P_s^* = 0.5[A_1 + A_{N/2+1}] + \sum_{i=2}^{N/2} A_i \quad (9)$$

and the total spectral power is given by

$$P_s \approx P_s^*/R'N. \quad (10)$$

The non-dimensional values of  $A_i$  are defined as

$$a_i = A_i/P_s^*. \quad (11)$$

Then the area under the non-dimensionalized spectral density versus frequency curve between the frequencies given by  $(m - 1)R'/N$  and  $(n - 1)R'/N$  gives the fraction of total spectral power contained between those frequencies. This non-dimensional spectral density is used to present the distribution of spectral energy. Similar non-dimensionalized power spectral densities may be used to study the interference effects in bubbly mixtures in a manner similar to that of Arakeri & Shanmuganathan (1985).



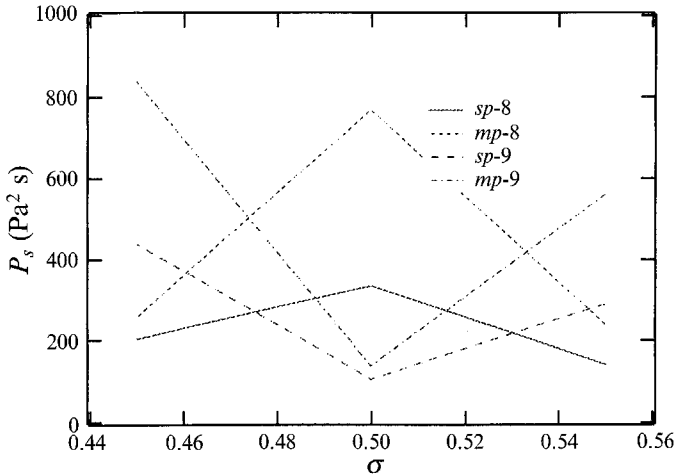


FIGURE 16. The total spectral power,  $P_s$ , plotted against the cavitation number for different types of events and the flow velocities (see legend). Data are for the ITTC headform.

The error in the spectra calculation is estimated using the methods of Bendat & Piersol (1980) in which the normalized standard error,  $\epsilon$  is given by

$$\epsilon = 1/\eta^{\frac{1}{2}}, \quad (12)$$

where  $\eta$  is number of data sets used to calculate the average power spectra. The bias error in the calculation is assumed to be negligible. With a 95% confidence level, the percentage limits on the average value of power spectra are approximately given by  $100.0/[1 \pm 2\epsilon]$ . Maximum uncertainty in the spectral density lies between 15% and 40% in most cases. More detailed errors are listed in Kumar (1991). The total spectral power and the non-dimensional spectral density will have the same maximum uncertainty. Thus the differences shown in figures 19–23 are meaningful since the uncertainty is around 30% in most cases while the differences in the spectra are in orders of magnitude.

We shall first examine the variation in the total spectral power with the type of event and with flow conditions for the two headforms. The total spectral power,  $P_s$ , is a measure of the sound energy emitted. The results for the ITTC headform (figure 16) reveal that  $P_s$  is larger for the *mp*-type events than for the *sp*-type events and does not show any consistent variation with flow velocity or cavitation number. On the other hand, for the Schiebe headform (figure 17),  $P_s$  decreases monotonically with increasing cavitation number and increases with increasing velocity. Again,  $P_s$  is generally larger for *mp*-type events than for *sp*-type events, though the difference is small at the larger cavitation numbers. The above results for  $P_s$  differ from the results for  $I_s$  explored earlier. However, it is important to recall that the total spectral power,  $P_s$ , contains the effects of reverberations from the water tunnel whereas  $I_s$  is a measure of the total spectral power in the acoustic pulse alone.

Non-dimensional spectral power densities were also calculated from the numerical solution of the Rayleigh–Plesset equation. The radiated acoustic pressure calculated from the volume oscillations of the bubble was used to obtain the power spectrum, which was non-dimensionalized in the same manner as the experimental records (equation (11)). A typical comparison of the non-dimensional spectral power density is shown in figure 18. The cavitation noise has a larger fraction of  $P_s$  emitted in the low-

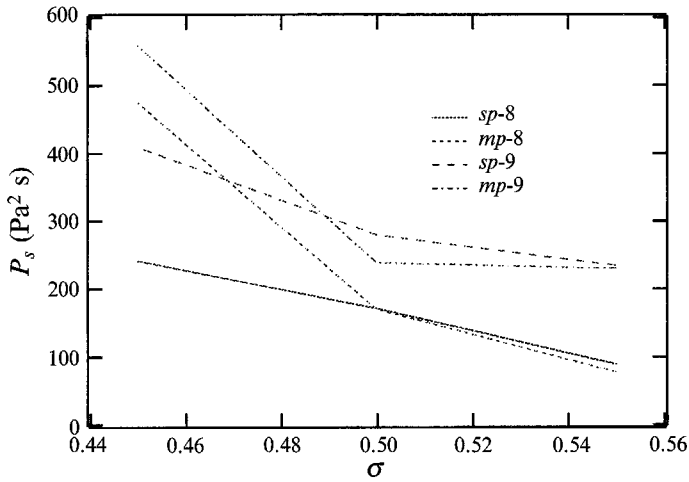


FIGURE 17. The total spectral power,  $P_s$ , plotted against the cavitation number for different types of events and the flow velocities (see legend). Data are for the Schiebe headform.

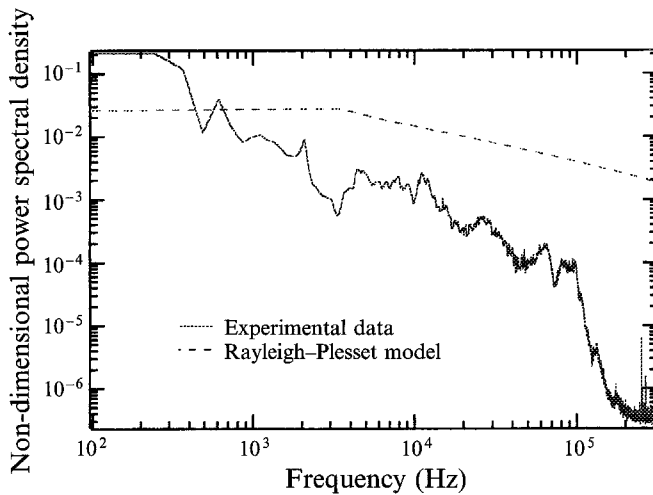


FIGURE 18. Typical non-dimensional power spectral density obtained from the experimental data for the Schiebe headform at  $\sigma = 0.45$  and flow velocity of 9 m/s. The superimposed spectrum is from the numerical calculations using the Rayleigh–Plesset equation for a 100  $\mu\text{m}$  nucleus in water tunnel conditions.

frequency region than do the Rayleigh–Plesset calculations. Consider some features of the experimental power spectrum. The spectrum decays as  $f^{-1.2}$  for frequencies less than 80 kHz. This suggests that no shock waves are detected by the hydrophone since their presence would be indicated by a  $f^{-2}$  decay in the spectra (Benjamin 1958). The decay of  $f^{-0.6}$ , a characteristic of the Rayleigh–Plesset calculations, is not seen in the experimental data. The reason for these discrepancies is probably the fact that the complex processes of bubble collapse in a flow are not adequately modelled by the Rayleigh–Plesset equation.

Changes in the non-dimensional power spectra were examined in order to understand the redistribution of the spectral energy due to changes in the cavitation number, the flow velocity, the type of event and the headform. Some of the significant results are

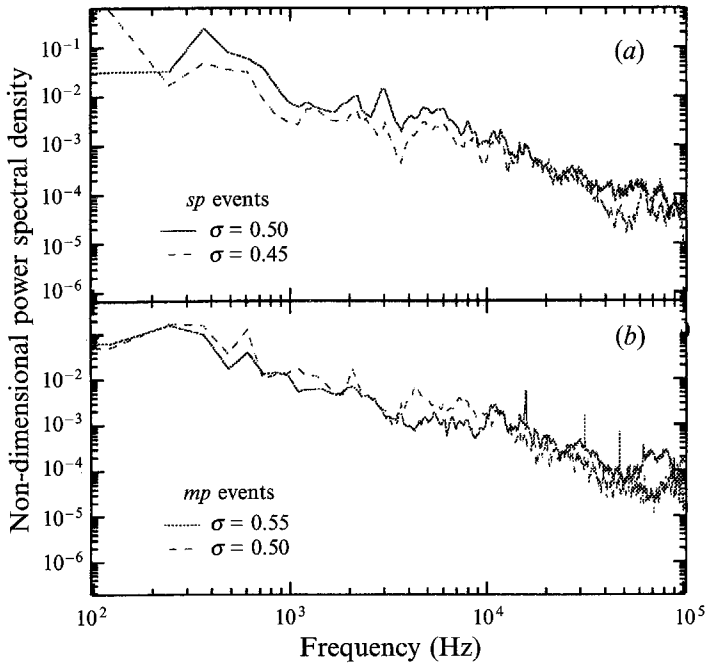


FIGURE 19. Effect of reduction in the cavitation number on the non-dimensional power spectral density. Experimental results for (a) the ITTC and (b) the Schiebe headform are shown here, at a flow velocity of 8 m/s.

shown in figures 19–23 and discussed below. Detailed results are given in Kumar (1991).

The changes in non-dimensional spectral density due to reduction in the cavitation number are shown in figure 19 for the ITTC and the Schiebe headforms. The spectral energy of the cavitation events on the ITTC headform shifts from higher to lower frequencies as the cavitation number is reduced. In particular, the spectral energy contained between the frequencies of 30 and 60 kHz is significantly reduced. Note that the peak separation,  $\tau_s$ , also increases from 15  $\mu\text{s}$  ( $1/66 \text{ kHz}^{-1}$ ) to 28  $\mu\text{s}$  ( $1/36 \text{ kHz}^{-1}$ ) with the same reduction in the cavitation number, which suggests that changes in the spectral energy distribution and the *effective width* of the acoustic pulse represented by the peak separation,  $\tau_s$ , are correlated. For *mp*-type events on the Schiebe headform, the spectral energy is transferred from high frequencies to medium frequencies and the fraction of spectral energy contained between the frequencies of 50 and 80 kHz is significantly reduced. However, these changes do not appear related to the variation in the peak separation.

The spectral energy distribution is not affected by the multi-peaking except in a few cases for the Schiebe headform. Figure 20 shows a typical comparison between the non-dimensional spectra for *sp*- and *mp*-type events on the Schiebe headform. It appears that spectral energy is transferred from the high frequencies to medium frequencies as a result of the multi-peaking. In particular, the reduction of the fraction of spectral energy contained between the frequencies of 50 and 75 kHz is significant. Such a reduction may be caused by the increase in the effective width of the acoustic pulse as a result of the multi-peaking.

The effect of flow velocity on the non-dimensional spectral density is examined next (figure 21). For low-cavitation-number events on the ITTC headform, the spectral

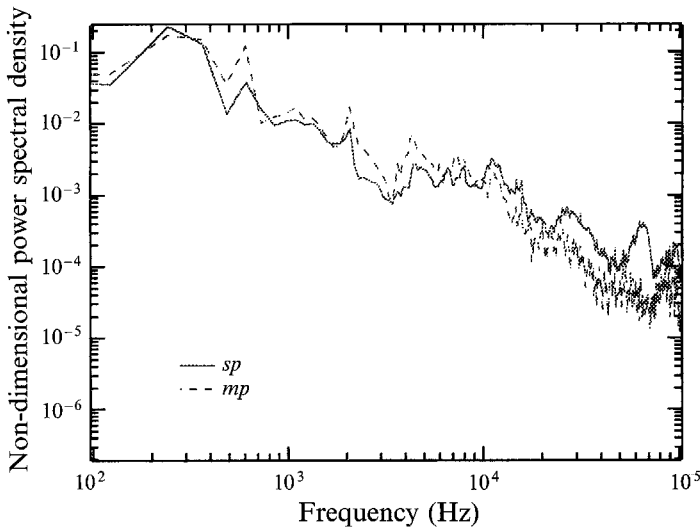


FIGURE 20. Effect of multipeaking on the non-dimensional power spectral density. Experimental data for the Schiebe headform at  $\sigma = 0.50$  and flow velocity of 8 m/s.

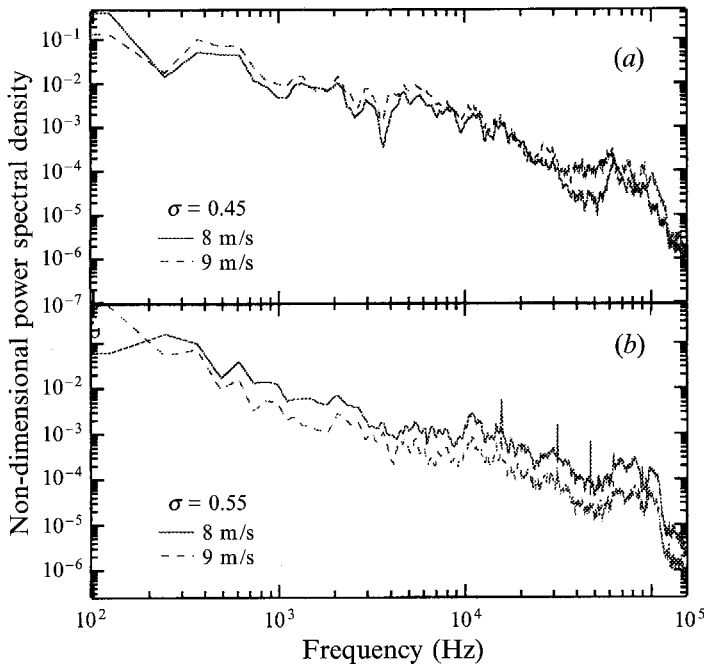


FIGURE 21. Effect of flow velocity on the non-dimensional power spectral density. Experimental data for (a) the ITTC and (b) the Schiebe headforms are shown here, for *mp* events.

energy is transferred from low frequencies to medium and high frequencies as a result of increase in the flow velocity. The fraction of spectral energy contained between 25 and 65 kHz is observed to be significantly increased by the increase in the flow velocity. On the other hand, the spectral energy is transferred from high and medium frequencies to very low frequencies with increase in the flow velocity for the events on the Schiebe headform. The extent of this energy transfer decreases with the reduction

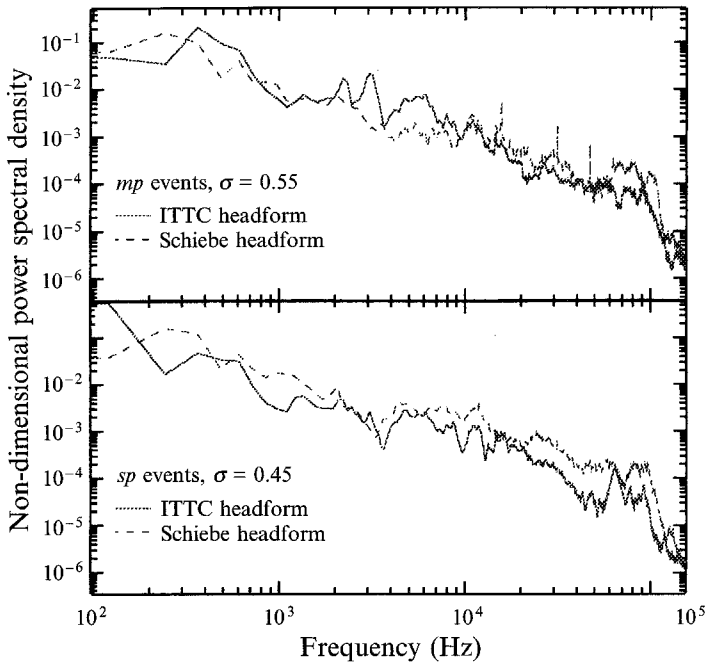


FIGURE 22. Comparison of the non-dimensional power spectral density for the ITTC and the Schiebe headforms, at a flow velocity of 8 m/s.

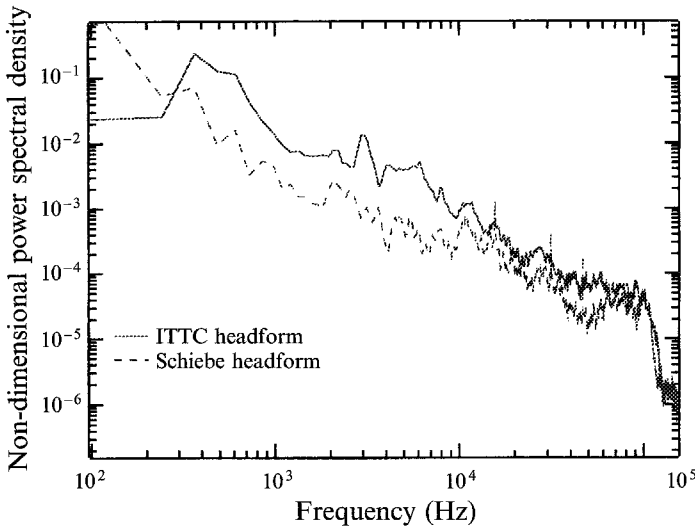


FIGURE 23. Comparison of the non-dimensional power spectral density for the ITTC and the Schiebe headforms. Experimental data for *mp*-type events, flow velocity of 9 m/s and cavitation number of 0.55.

in cavitation number. The reasons for these changes in the spectral energy distribution are not understood.

The non-dimensional spectral densities for the two headforms are compared next (figure 22). At the flow velocity of 8 m/s, the Schiebe headform has a larger fraction of the spectral energy in the low-frequency range compared with the ITTC headform at the cavitation number of 0.55. As the cavitation number is reduced to 0.45, the

Schiebe headform contains a smaller fraction of the spectral energy in the low-frequency range compared with the ITTC headform. In contrast, the Schiebe headform has a larger fraction of the spectral energy in the low-frequency range at the flow velocity of 9 m/s (figure 23). The reasons for these changes in the spectral energy distributions are not understood.

#### 4. Summary and conclusions

In the present experiments on travelling bubble cavitation around axisymmetric headforms, the cavitation bubbles were seen to collapse, rebound and collapse again resulting in an acoustic signal consisting of two pulses, a phenomena known as rebounding. Each of the pulses in the acoustic signal produced by a single cavitation even may contain more than one peak. This is called multipeaking. The occurrence of rebounding and multipeaking and their impact on some of the characteristic measures of the acoustic signal such as the spectra have been investigated in order to learn more about the process of cavitation bubble collapse and about sound emission in travelling bubble cavitation.

It is observed that for the ITTC headform, multipeaking and rebounding increase with reduction in the cavitation number. However, for the Schiebe headform, multipeaking decreases and rebounding increases as the cavitation number is reduced. The flow velocity seems to have little effect on these results though only small changes in the flow velocity were possible. In the case of the Schiebe headform most events with a rebound produced single-peaked acoustic pulses, whereas, in case of the ITTC headform, most events produced a multipeaked pulse from the first collapse followed by a single-peaked pulse from the second collapse. Natural oscillations of the collapsing bubble seem the most likely cause of multipeaked pulses. The ratio of peak amplitude of the main pulse to the peak amplitude of the rebound pulse is close to 2.0 for all flow conditions and types of events. This may indicate a fairly repeatable process of bubble fission and rebound. Some factors such as smaller cavitation number, smaller flow velocity and multipeaking are seen to delay the rebound.

Other features of the single-bubble acoustic output such as the peak pressure, the acoustic impulse and the pulse width were examined in order to understand the effect of changes in cavitation number, flow velocity and local flow structure. It was found that all of these except the pulse width,  $\tau_w$ , increased significantly in magnitude with the reduction in cavitation number. Multipeaking and rebounding were also observed to increase the magnitude of these acoustic characteristics. The peak separation,  $\tau_s$ , was practically constant at 12  $\mu\text{s}$  for the Schiebe headform but increased from 15 to 23–28  $\mu\text{s}$  with reduction in the cavitation number for the ITTC headform.

Theoretical investigations based on the Rayleigh–Plesset equation predicted the right order of magnitude for the acoustic characteristics but failed to predict the dependence of the pulse width on cavitation number. The theory does not adequately predict the distribution of spectral energy.

The fraction of spectral energy contained in the high-frequency range (30–80 kHz) is reduced by the reduction in the cavitation number. This appears correlated to an increase in effective width of the pulse represented by peak separation,  $\tau_s$ , for the ITTC headform. A similar reduction in the fraction of the spectral energy contained in high frequencies occurs for the Schiebe headform due to multipeaking. This may also be due to an increase in the effective width of the acoustic signal caused by multipeaking.

An increase in the flow velocity increases the fraction of spectral energy contained in the high frequencies for the ITTC headform. However, the effect is just the reverse

for the Schiebe headform, for which the fraction of spectral energy contained in high frequencies is reduced by an increase in the flow velocity.

The authors are grateful for the support of Office of Naval Research under contract N000167-85-K-0165. We thank Professors Allan J. Acosta and Steven L. Ceccio and graduate students, Yan Kuhn de Chizelle and Douglas Hart for their advice and assistance. The authors are also grateful to the reviewers for their helpful comments and suggestions included in the paper.

#### REFERENCES

- ARAKERI, V. H. & SHANMUGANATHAN, V. 1985 On the evidence for the effect of bubble interference on cavitation noise. *J. Fluid Mech.* **159**, 130–150.
- BAITER, H. J. 1974 Aspects of cavitation noise. In *Symp. on High Powered Propulsion of Ships, Wageningen, The Netherlands, Publication 490*, pp. 1–39.
- BAITER, H. J. 1982 Estimates of acoustic efficiency of collapsing bubbles. In *Intl. Symp. on Cavitation Noise, ASME Book H00231*, pp. 35–44.
- BAITER, H. J. 1986 On different notions of cavitation noise and what they imply. In *Intl Symp. on Cavitation and Multiphase Flow Noise, ASME, FED Vol. 45*, pp. 107–118.
- BENDAT, J. S. & PIERSOL, A. G. 1971 *Measurement and Analysis of Random Data*. John Wiley and Sons.
- BENDAT, J. S. & PIERSOL, A. G. 1980 *Engineering Applications of Correlation and Spectral Analysis*. John Wiley and sons.
- BENJAMIN, T. B. 1958 Pressure waves from collapsing cavities. In *Second ONR Symp. on Naval Hydrodynamics* (ed. R. D. Cooper), pp. 207–233.
- BENJAMIN, T. B. & ELLIS, A. T. 1966 The collapse of cavitation bubbles and the pressures thereby produced against solid boundaries. *Phil. Trans. R. Soc. Lond. A* **260**, 221–240.
- BLAKE, J. R., TAIB, B. B. & DOHERTY, G. 1986 Transient cavities near boundaries. Part 1. Rigid boundary. *J. Fluid Mech.* **170**, 479–497.
- BLAKE, W. K., WOLPERT, M. J. & GEIB, F. E. 1977 Cavitation noise and inception as influenced by boundary layer development on a hydrofoil. *J. Fluid Mech.* **80**, 617–640.
- BRENNEN, C. E. & CECCIO, S. L. 1989 Recent observations on cavitation and cavitation noise. In *Proc. Third Intl Symp. on Cav. Noise and Erosion in Fluid Systems, San Francisco, Ca*, pp. 67–78. ASME.
- CECCIO, S. L. 1990 Observations of the dynamics and the acoustic of travelling bubble cavitation. PhD thesis, California Institute of Technology.
- CECCIO, S. L. & BRENNEN, C. E. 1991 The dynamics and acoustics of travelling bubble cavitation. *J. Fluid Mech.* **233**, 633–660.
- ELLIS, A. T. 1952 Observations on cavitation bubble collapse. *Rep.* 21–12. California Institute of Technology, Hydrodynamics Laboratory.
- FITZPATRICK, H. M. & STRASBERG, M. 1956 Hydrodynamic sources of sound. In *First Symp. on Naval Hydrodynamics, Washington DC*, pp. 241–280.
- FLYNN, H. G. 1964 Physics of acoustic cavitation in liquids. In *Physical Acoustics: Principles and Methods*, vol. 1, part B (ed. W. P. Mason), pp. 57–172. Academic.
- GATES, E. M. 1977 The influence of freestream turbulence, freestream nuclei populations and drag reducing polymer on cavitation inception on two axisymmetric bodies. *Rep.* E182-2. California Institute of Technology Division of Engineering and Applied Science.
- GATES, E. M., BILLET, M. L., KATZ, J., OOI, K. K., HOLL, W. & ACOSTA, A. J. 1979 Cavitation inception and nuclei distribution – joint ARL–CIT experiments. *Rep.* E244-1, California Institute of Technology, Hydrodynamics Laboratory.
- GILMORE, F. R. 1952 The growth and collapse of a spherical bubble in a viscous compressible liquid. *Hydrodynamics Laboratory Rep.* 26–4. California Institute of Technology.
- HAMILTON, M. F. 1981 Travelling bubble cavitation and resulting noise. *Appl. Res. Lab. Tech. Mem.* TM 81–76. Pennsylvania State University.

- HAMILTON, M. F., THOMPSON, D. E. & BILLET, M. L. 1982 An experimental study of travelling bubble cavitation and noise. In *Intl. Symp. on Cavitation Noise*, pp. 25–32. ASME.
- HARRISON, M. 1952 An experimental study of single bubble cavitation noise. *J. Acoust. Soc. Am.* **24**, 776–782.
- HOYT, J. W. 1966 Wall effect on the ITTC standard head shape pressure distribution. In *11th Intl Towing Tank Conf., Tokyo, April 1966*.
- ILICHEV, V. I. & LESUNOVSKII, V. P. 1963 On noise spectra associated with hydrodynamic cavitation. *Sov. Phys.-Acoust.* **9**, 25–28.
- KIMOTO, H. 1987 An experimental evaluation of the effects of a water microjet and a shock wave by a local pressure sensor. In *Intl Symp. on Cavitation Research Facilities and Techniques, ASME FED* vol. 57, pp. 217–224.
- KNAPP, R. T. & HOLLANDER, A. 1948 *Laboratory investigations of the mechanisms of cavitation. Trans. ASME*, July, pp. 419–435.
- KUMAR, S. 1991 Some theoretical and experimental studies of cavitation noise. PhD thesis, California Institute of Technology.
- KUHN DE CHIZELLE, Y. 1993 The hydrodynamics, acoustics and scaling of travelling bubble cavitation. PhD thesis, California Institute of Technology.
- KUHN DE CHIZELLE, Y., CECCIO, S. L., BRENNEN, C. E. & GOWING, S. 1992 Scaling experiments on the dynamics and acoustics of travelling bubble cavitation. *Proc. Conf. on Cavitation, Cambridge, England, Dec. 1992*.
- LAUTERBORN, W. & BOLLE, H. 1975 Experimental investigation of cavitation bubble collapse in the neighbourhood of a solid boundary. *J. Fluid Mech.* **72**, 391–399.
- LINDGREN, H. & JOHNSON, C. A. 1966 Cavitation inception on headforms – ITTC comparative experiments. *11th Intl Tank Towing. Conf. Tokyo, 1966*, pp. 219–232. (Also Publications of the Swedish State Shipbuilding Experimental Tank, No. 58, 1966.)
- MARBOE, M. L., BILLET, M. L. & THOMPSON, D. E. 1986 Some aspects of travelling bubble cavitation and noise. *Intl Symp. on Cavitation and Multiphase Flow Noise, ASME FED.* **45**, 119–126.
- MELLEN, R. H. 1954 Ultrasonic spectrum of cavitation noise in water. *J. Acoust. Soc. Am.* **26**, 356–360.
- MELLEN, R. H. 1956 An experimental study of the collapse of a spherical cavity in water. *J. Acoust. Soc. Am.* **28**, 447–454.
- MEULEN, J. H. J. VAN DER & RENESSE, R. L. VAN 1989 The collapse of bubbles in a flow near a boundary *17th Symp. on Naval Hydrodynamics, The Hague*, pp. 379–391.
- MORZOV, V. P. 1969 Cavitation noise as a train of pulses generated at random times. *Sov. Phys. Acoust.* **14**, 361–365.
- NAUDÉ, C. F. & ELLIS, A. T. 1961 On the mechanism of cavitation damage by nonhemispherical cavities collapsing in contact with a solid boundary. *Trans. ASME D: J. Basic Engng* **83**, 648–656.
- PLESSET, M. S. & CHAPMAN, R. B. 1971 Collapse of an initially spherical cavity in neighbourhood of a solid boundary. *J. Fluid Mech.* **47**, 283–290.
- PLESSET, M. S. & PROSPERETTI, A. 1977 Bubble dynamics and cavitation. *Ann. Rev. Fluid Mech.* **9**, 145–185.
- SCHIEBE, F. R. 1972 Measurement of the cavitation susceptibility of water using standard bodies. *St. Anthony Falls Hydraulic Laboratory, University of Minnesota, Rep.* 118.
- TESLENKO, V. S. 1980 Experimental investigations of bubble collapse at laser-induced breakdown in liquids. In *Cavitation and Inhomogeneities in Underwater Acoustics, Proc. First Int. Conf.* (ed. W. Lauterborn), pp. 30–34. Springer.
- VOGEL, A., LAUTERBORN, W. & TIMM, R. 1989 Optical and acoustic investigations of dynamics of the laser-produced cavitation bubbles near a solid boundary. *J. Fluid Mech.* **206**, 299–338.